18A.6
RAMAN-SHIFTED EYE-SAFE AEROSOL LIDAR (REAL) OBSERVATIONS DURING THE CANOPY HORIZONTAL ARRAY TURBULENCE STUDY (CHATS)

Shane D. Mayor[*]

National Center for Atmospheric Research, Boulder, Colorado, USA

1. MOTIVATION

The activity of scanning an elastic backscatter lidar to observe the internal structure and motion of the atmospheric boundary layer deserves to be explored again in order to determine if recent improvements in eye-safety and analog direct-detection at 1.5 microns wavelength can yield any new information that may have been difficult or impossible to extract from data collected with previous generations of elastic lidars. In particular, the inability until recently to safely and reliably transmit high pulse energy is likely to have subdued interest and enthusiasm in exploring the limits of fine-scale quantitative information that can be extracted from elastic lidar data. These measurements may include quantities such as the radial and tangential components of motion, eddy structure and lifetime. (See Kunkel et al. (1980) and Mayor et al. (2003) for examples of previous work in this area).

In recent decades, eye-safe scanning coherent Doppler lidars have made significant strides and contributions in boundary layer meteorology. However, they have limitations. For example, they can only detect the radial component of the velocity field and lack the performance necessary to detect very small variations in the aerosol backscatter intensity. The range resolution of coherent Doppler lidars is also restricted. These are fundamental limitations due to the requirement of implementing the heterodyne detection technique in order to detect the Doppler phase shift caused by the advection of particles.

The hypothesis for the present work is that coherent turbulent motions (ejections, sweeps, streaks, etc.) in the roughness sublayer during fair-weather conditions may in many cases modulate the aerosol backscattering field sufficiently to cause a detectable change in lidar backscatter. The ability to make 2-dimensional images and time-lapse animations of such flow features would be useful for example in testing large eddy simulations or studying the effect of such motions on the dispersion of particulate matter. Extending elastic lidar cor-

[*]*corresponding author address:* Shane D. Mayor, Ph.D., National Center for Atmospheric Research, P. O. Box 3000, Boulder, CO, 80307-3000; *email*: sdmayor@gmail.com. After mid-August, 2008: California State University at Chico, Chico, California, 95929.

Figure 1: The REAL as deployed for CHATS.

relation methods (Eloranta et al., 1975; Sasano et al., 1982; Mayor and Eloranta, 2001) to resolve finer scales of the radial and tangential components of turbulent motion would also be useful. For example, applying this technique to shallow RHI scans may allow one to determine horizontal and vertical velocities in the surface layer simultaneously.

In addition, eye-safety allows the lidar to scan more closely to the surface than previous investigators may have felt comfortable doing, and eye-safety encourages unattended and 24/7 operation. This leads to a substantial improvement in sampling capability. This paper briefly describes the instrument, experiment, preliminary instrument performance results, and some highlights of observations from the experiment. It concludes with suggestions for future activities.

2. EXPERIMENT

The Raman-shifted Eye-safe Aerosol Lidar (REAL) was deployed during the Canopy Horizontal Array Turbulence Study (CHATS) field experiment from 15 March through 11 June 2007 in Dixon, California. The purpose of the deployment was (a) to test the lidar's ability to create two-dimensional images and time-lapse animations of fine-scale turbulent coherent structures just above canopy level from inhomogeneities in the aerosol optical backscattering and (b) to provide observations of the atmospheric boundary layer over and around the heavily instrumented tower sites embedded within the canopy.

Wavelength	1.543 microns
Pulse energy	170 mJ
Pulse rate	10 Hz
Pulse duration	6 ns
Beam diameter at BSU	66 mm ($1/e^2$ FWHM)
Beam divergence	0.24 mrad (full-angle)
Telescope dia.	40 cm
Receiver FOV	0.54 mrad (full-angle)
Digitizer speed	100 MHz
Digitizer range	14 bits
Detector type	200-μm InGaAs APD

Table 1: Parameters of the lidar system

The REAL is described in detail by Mayor and Spuler (2004) and Spuler and Mayor (2005). The lidar is unique in that it operates at 1.5-microns wavelength with high-pulse energy. This wavelength falls within a narrow region of the near-infrared portion of the optical spectrum that offers maximum eye-safety. By operating at this wavelength, a lidar can safely transmit pulses with sufficient energy to see several kilometers from a single pulse. REAL is eye-safe at 0 meters range for a 10 second unaided stare according to ANSI standards. An additional important feature for lidar operation in urban regions is an invisible beam. Other eye-safe lidars with invisible beams exist, but high-pulse energy operation at 1.5 microns enables use of an analog direct detection receiver and rapid scanning. Rapid scanning enables one to create time-lapse animations of flow as evidenced by variability in the aerosol backscatter. The system, as configured for CHATS, transmitted 10 laser pulses per second.

Just prior to the deployment to CHATS, REAL benefited from several substantial improvements. They include (1) the ability to run continuously and unattended for periods of several weeks, (2) the ability to interleave the collection RHI and PPI scans in order to provide horizontal and vertical animations during the same period, (3) backscatter polarization sensitivity* (Mayor et al., 2007b), and (4) remote control and near-real-time perusal of "Quick-look" scan images via the internet. Final data products are now delivered in NetCDF format and programs have been written in Matlab and IDL to make data access and custom data processing easier. Analog to digital signal processing rates were increased to 100 million samples per second for CHATS in order to record backscatter at 1.5-meter intervals. Detection signal amplifier electronics were rebuilt in an effort to increase receiver bandwidth and sense finer scale variability along the beam.

The REAL was installed among a wide variety of agricultural fields approximately 5 kilometers north of the

---

*REAL was not operated in the polarization sensitive mode for CHATS.

Figure 2: The CHATS site was located approximately 100 km from the Pacific Ocean—a source of marine air. Well-defined sea-breeze fronts passed over the site on at least 4 separate occasions during the 3 month deployment. An example of one sea-breeze front is presented in Section 3.4.

city of Dixon, California (see Fig. 2 and 3). The site was chosen for its exceptional flatness and clear vantage of the northern edge of a very large walnut orchard located 1.4 km to the south. Arrays of in situ sensors were installed on towers in the orchard in order to investigate the interaction of boundary-layer scale fluid mechanics and the canopy-imposed influences on momentum and scalar exchange. Therefore, the main observation site in CHATS was a custom tower structure supporting horizontal arrays of closely spaced in situ sensors located in the orchard about 1.71 km from the lidar. The structure supporting the arrays was 12 meters tall. Additionally, a 30 meter tall tower was located 1.61 km from the lidar site. Trees in the orchard were approximately 10 meters tall. This location allowed the lidar to routinely make PPI scans at elevation angles as low as 0.2 degrees above horizontal without interference from the orchard trees.

3. OBSERVATIONS

The lidar was operated nearly continuously and unattended at CHATS from 15 March to 11 June, 2007. Visits by staff every few weeks were made to change laser flashlamps and hard disks. Only a few interruptions lasting more than an hour, and sometimes as long as a few days, occurred due to electrical power disruptions and, in one case, failure of a commercial digitizer card. The result of the deployment is very large data set—containing over 2.5 TB of raw data from over 1850 hours of operation. The lidar is equipped with a precipitation sensor in

Figure 3: Looking south over the CHATS site as photographed by Carlye Calvin from the Duke University helicopter. The REAL is located at the bottom center of the picture.
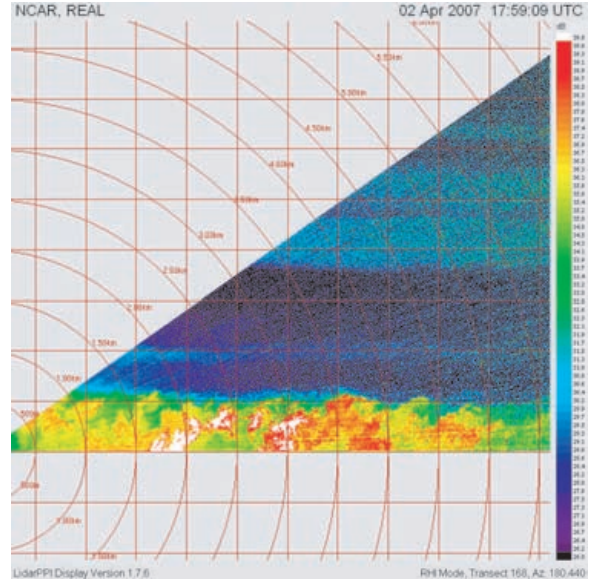

Figure 4: Range versus height image of aerosol backscatter from a single scan through a convective boundary layer at 17:59:09 UTC on 2 April 2007 at CHATS.

order suspend operations during rain events.

A variety of scan strategies were conducted with the lidar during the experiment. Since the primary goal was to observe very fine-scale turbulent coherent structures over the orchard, the lidar was often programmed to make narrow RHI and PPI scans directly over the orchard. However, because ideal conditions for the in situ component of the experiment only occurred when the wind was from the south, wide-angle RHI and PPI scans were collected at other times. In many cases, RHI and PPI scans were collected in a continuously alternating fashion so that time-lapse animations of both horizontal and vertical atmospheric structure could be obtained simultaneously. In addition to scanning, the beam was periodically pointed toward a position near the tower and held stationary for a period of a few minutes to record fixed beam data.

Figures 4 and 5 are just two examples of typical vertical scans collected during turbulent and non-turbulent conditions, respectively. Data to approximately 0 to 5.6 km range on the horizontal axis are shown. Each of these scans required less than 15 seconds to acquire. The lidar typically observed a large amount of horizontal inhomogeneity during turbulent daytime conditions. This is likely due to agricultural operations and the inhomogeneous surface which provided an abundance of wind blown soil or pollen particles. The aerosol backscatter tends to be horizontally homogeneous during stable and very low wind-speed conditions that typically occurred at night and as shown in Fig. 5.

The quantity shown in Figs. 4 and 5 is *relative* aerosol backscatter in decibels (dB). To arrive at these values, the background level was subtracted from the raw digitizer counts on a shot-to-shot basis and the waveforms are corrected for the $1/r^2$ shape common to all direct-

detection lidar signals. The data are then converted to dB by taking the $\log_{10}$ of the result and multiplying by 10. These data are not corrected for pulse-to-pulse energy variations or attenuation. Warmer colors are indicative of higher optical scattering caused by an increase in particle concentration, a shift towards a larger size distribution of particles, or of particles that backscatter radiation at 1.5 microns more efficiently.

3.1 Signal-to-noise ratio

Detecting fine-scale turbulent coherent atmospheric structures in aerosol backscatter data depends critically on generating high signal-to-noise ratio backscatter data and simultaneously achieving high spatial and temporal resolution. Fig. 6 presents backscatter data as a function of range resulting from a single laser pulse during a period when the aerosol backscattering was horizontally homogeneous and strong in intensity. (The shot was taken within 20 seconds of the completion of the RHI scan shown in Fig. 5 and when the beam was directed at an elevation angle of 0.2016° and an azimuth angle of 180.473°.) Each panel in Fig. 6 is a different way of looking at the same result. In the top panel, 6A, the original backscatter signal is shown with linear axes and in units of digitizer counts. This was obtained by adding the signals from the parallel and perpendicular receiver channels at each range and subtracting the average background signal based on several hundred points prior to laser discharge. The main characteristic to notice in 6A
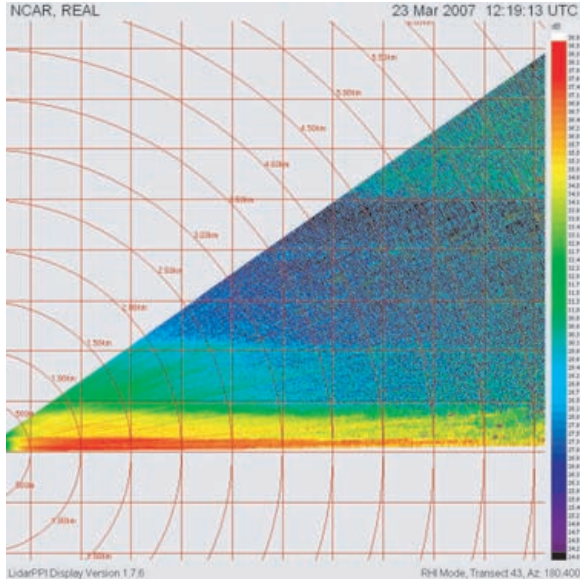
Figure 5: Range versus height image of aerosol backscatter from a single scan through a stable boundary layer at 12:19:13 UTC on 23 March 2007 at CHATS.

is the large dynamic range due to the $1/r^2$ nature of the lidar signal. This makes the detection of coherent structures more difficult with increasing range. In panel 6B, signal-to-noise ratio is presented. This was obtained by calculating the standard deviation of the background (i.e. the data prior to laser discharge) and dividing the signal shown in 6A by this constant amount. The key point to note from 6B is that the aerosol backscatter signal is over 100 times larger than the noise level of the detection electronics at ranges of about 1 km and remains at least 10 times larger out to ranges of approximately 5 km. Fig. 6C shows the relative aerosol backscattering in dB, corrected for the $1/r^2$ effect but not corrected for attenuation. This is the same quantity as shown in the images in Figs. 4 and 5. It confirms that the aerosol backscattering from this period is indeed homogeneous as a function of range—lacking significant coherent aerosol structures as intended by choosing this particular period of time. The absolute magnitude of the data in Fig. 6C isn't meaningful since it may change as the result of instrument performance or aerosol backscattering efficiency and extinction. Rather, it is the range in intensity variations that will be discussed. Towards that, 6D shows the high-pass median filtered version of 6C. Here any coherent aerosol features larger than about 333 range gates (500 m length) would be removed. Fig. 6D shows the minimum intensity magnitude that variations caused by turbulent coherent structures must exceed in order for the lidar to detect above the noise background. In this particular case, it is less than about ±0.25 dB at 500 m range

and increases to ±1 dB at approximately 5 km range. These values in dB correspond to changes in backscatter intensity of $\pm5.9\%$ and $\pm25.9\%$, respectively. Aerosol features smaller than 500 m length and having intensity changes of more than these amounts should be detectable. If the average aerosol backscatter intensity were to change, this result would also change at a given range. In future work, it is possible to calculate this threshold as a function of average SNR and show how many particles of a given size distribution correspond to such small changes in lidar signal intensity.
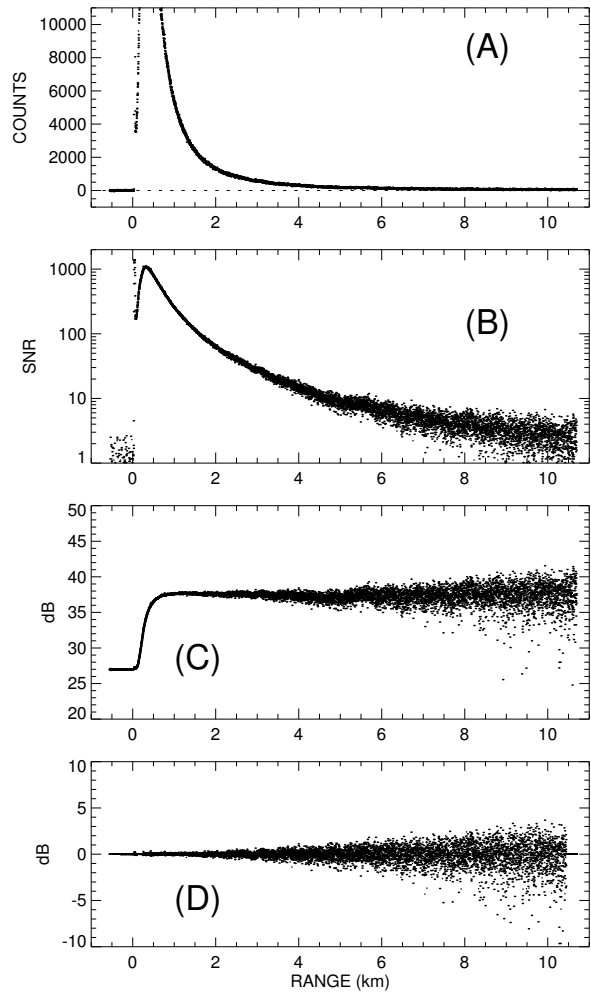

Figure 6: Results from a single pulse pointed almost horizontally at 12:19:32.2340 UTC on 23 March 2007. (A) Original signal before $1/r^2$ correction. (B) Signal-to-noise ratio of original signal. (C) Backscatter after correction for $1/r^2$ trend. (D) High-pass median filtered version of C.
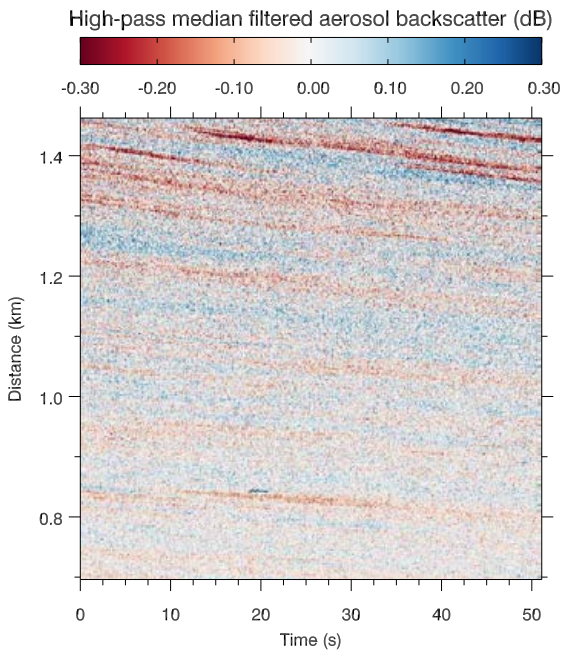
High-pass median filtered aerosol backscatter (dB)

Figure 7: Time versus range image of high-pass median filtered aerosol backscatter during a period when the beam was held stationary and almost horizontal. This period was selected for it's uniformity and good SNR in order to explore the spatial and temporal resolution of the instrument. These data were used to compute the autocorrelation functions shown in Fig. 8. The data were collected on 10:15:47.125 to 10:16:38.218 UTC on 25 May 2007 and spanned 696 m to 1462 m range.

3.2   Resolution

Backscatter data were saved at 1.5 m spatial and 0.1 s temporal intervals. However, the resolution of the lidar data can be limited by unwanted correlations in the backscatter signal. Such undesirable correlations may be caused by excessive laser pulse length, amplifier bandwidth, or other system limitations and errors. As the distance or time between independent data points becomes smaller, the ability to resolve finer-scale atmospheric structures increases. To show the statistical independence of backscatter sample points, data from a period when the beam was pointing almost horizontally (180.438° azimuth and 0.0495° elevation) and stationary was subjected to autocorrelation analysis. As in section 3.1, a period of time when the atmospheric backscatter appeared to be uniform and exhibited strong SNR was chosen (see Fig. 7). Backscatter variations in the atmosphere will also introduce correlations. By selecting a period with uniform backscattering, it is possible to highlight instrument-induced correlations. Backscatter from 512 consecutive laser pulses and spanning 512

consecutive points in range were chosen. The range spanned from 696 m to 1462 m and the time spanned from 10:15:47.125 to 10:16:38.218 UTC. The SNR of these points ranged from over 500 to approximately 90. During this time in the experiment, data beyond 1452 m were contaminated by backscatter from the beam grazing the top of the orchard trees.
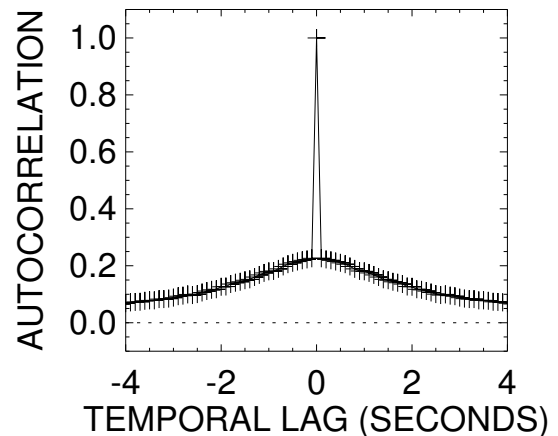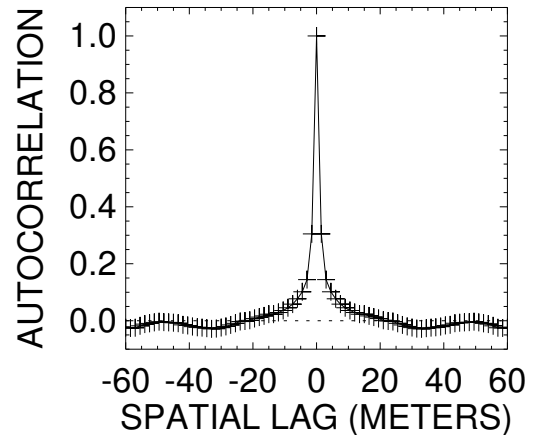

Figure 8: Spatial (top) and temporal (bottom) autocorrelation functions for high-pass median filtered aerosol backscatter data between 696 and 1462 m range during a 51.2 s horizontal stare that began at 10:15:47.125 UTC on 25 May 2007.

The top panel of Fig. 8 shows the spatial autocorrelation function. This represents correlations of signal with itself along the beam. It shows that the lidar signal is highly de-correlated (i.e. <0.20) within ±3 m of itself in range. The autocorrelation function crosses 0 at approximately ±20 m lag. The bottom panel of Fig. 8 shows the temporal autocorrelation function. This represents cor-

relations at a given range with the same range in subsequent pulses. Again, the signal is very decorrelated (i.e. <0.25) with itself at 0.1 s lag (1 laser pulse). There is however, a broad pedestal of weak correlation that gently decreases with range. This is caused by fine-scale aerosol structures slowly (1–2 m s^{-1}) advecting through the beam during this 51.2 s period. The aerosol structures appear as sloped bands if Fig. 7.

3.3 Stable Boundary Layer

The images resulting from horizontal scans collected during the night at CHATS often reveal fine-scale wave activity. Applying numerical high-pass median filtering to the range-corrected backscatter signal better enables one to see the smaller scales ($<$ 1 km) of coherent structures. Although many hundreds of hours of data are available for analysis, only one 2.5 hour period is presented here to highlight how the lidar data can be used to gain an improved understanding of boundary layer events.

Fig. 9 shows the time-series of vertical velocity, wind speed, temperature and wind direction from a height of 12.5 m on the tower. The PPI scans shown in fig. 10 intersected the tower at this altitude. This 2.5 hour period occurred during the evening from 20:15 to 22:45 PST. In contrast to the unstable boundary layer shown in the next section, the z/L stability parameter at 12.5 m during this period was approximately + 0.035 indicating weakly stable stratification. The tower data traces show episodes of vertical mixing. For example, during the first 30 minutes vertical velocities approaching ± 1 m s^{-1} are observed followed by a very calm period from 4:45 to 5:27 UTC. This is followed by an abrupt episode of mixing. The turbulence occurred when the wind speed increased to approximately 2 m s^{-1}. At this point in time, the air temperature dropped by approximately 1°C. Within approximately 10 minutes the vertical velocities and wind speeds have reduced again.

Figs. 10(a), 10(b), and 10(c) show the lidar horizontal scans just prior, at the onset of, and during this event, respectively. Before the episode, the aerosol backscatter in the vicinity of the tower is homogeneous. The onset of turbulence occurs as a large positive perturbation of aerosol backscatter intensity begins advecting across the site from the southwest to the northeast. During the turbulent period, the aerosol backscatter exhibits significant small-scale variability. Presumably, higher wind speeds and turbulence are lifting particulate matter from the surface and foliage where it then serves as a tracer of the turbulent motions. It is also plausible that the turbulent region brings higher backscattering air with it. In any case, this region of disturbed backscatter extends beyond the edges of the scan. The lidar data shows that the fea-

ture causing the episode of turbulence advects across the tower at about the same speed as the wind speed and is large in scale—possibly a very shallow density current. Unfortunately, RHI scans during this period were only collected once per 12-minutes. This sample rate is insufficient to depict coherent motions of the aerosol features in a vertical plane.

3.4 Sea-breeze Fronts

Four well-defined sea-breeze fronts were observed during the approximately 3 month period of CHATS. In each case, marine airmasses containing aerosol particles that resulted in higher backscatter intensity advected over the site from the south in the presence of larger scale northerly flows. As shown in Fig. 2, the Pacific Ocean is approximately 100 km from the lidar site and accessible through the San Francisco Bay. Note also that all of the sea-breeze frontal passage events identified in the data set occurred in the afternoon.

For brevity only one of the four cases is presented here. Details of the other cases can be found in Mayor et al. (2007a, 2008). On 26 April the lidar was recording data to a maximum of 5.8-km range and collecting consecutively interleaved horizontal and vertical scans. A small selection of scans are shown in Figs. 11 and 12. The marine airmass, colored in red, exhibits approximately 3.5 dB higher aerosol backscatter signal than the environmental backscatter. The lidar shows that the front traveled 5.8 km in slightly less than 51 minutes, or an average speed of 1.9 m s^{-1}. RHI scans show that the airmass north of the front is turbulent with aerosol plumes reaching 1.5 km altitude. The RHI scans also show structures resembling Kelvin-Helmholtz billows shearing off the leading edge of the front and moving south. These billows reach altitudes over 1 km at distances of 1.5 to 2.0 km south of the leading edge of the front. The largest billows appear to have wavelengths on the order of 1 km. The lidar is uniquely capable of observing the speed of the leading edge of this density current and its vertical extent.

In situ time-series from sensors on the 30 m tall tower, shown in Fig. 13, indicate that the air temperature dropped by approximately 2°C and the relative humidity (not shown) increased by about 12% when this front passed over. The wind direction changed from northerly before the arrival of the front to southerly after the frontal passage. The wind speed during the hour surrounding the frontal passage did not exceed 5 m s^{-1} at the top of the tower. The z/L stability parameter at 12.5 m height ranged from -2.0 to -0.6 (strongly to moderately unstable) before the arrival of the front to -0.5 to -0.2 (moderately to weakly stable) after the passage of the front.
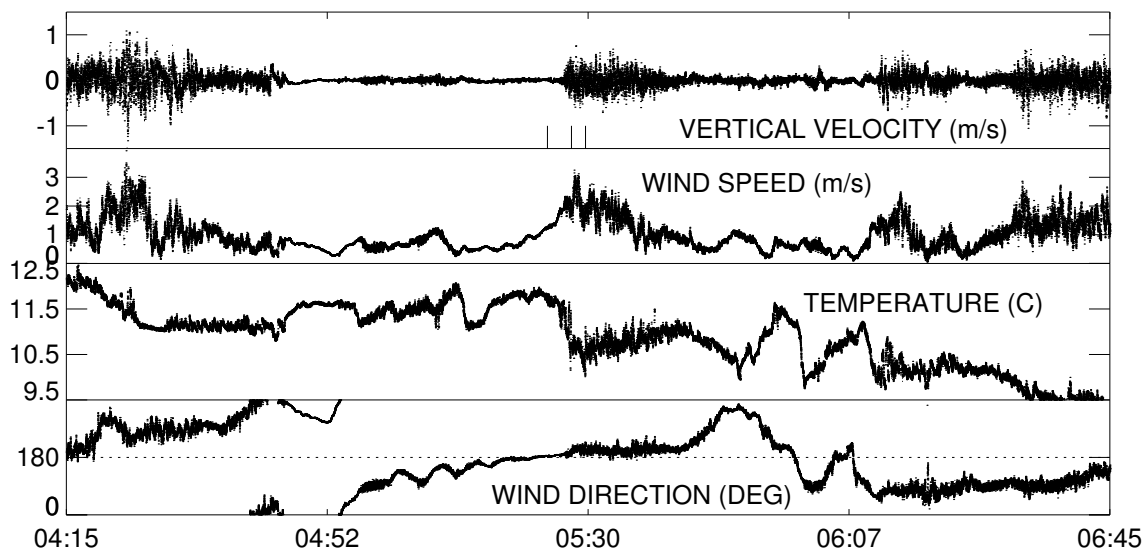
Figure 9: Time series of vertical velocity, horizontal wind speed, temperature, and wind direction collected from in situ sensors on a tower at 12.5 m above the ground during a stable evening boundary layer on 21 March 2007. These 6 Hz data were extracted from a 60 Hz time series. Times are in UTC. The three vertical lines near the middle of the top plot indicate the times of the frames shown in Fig.10.
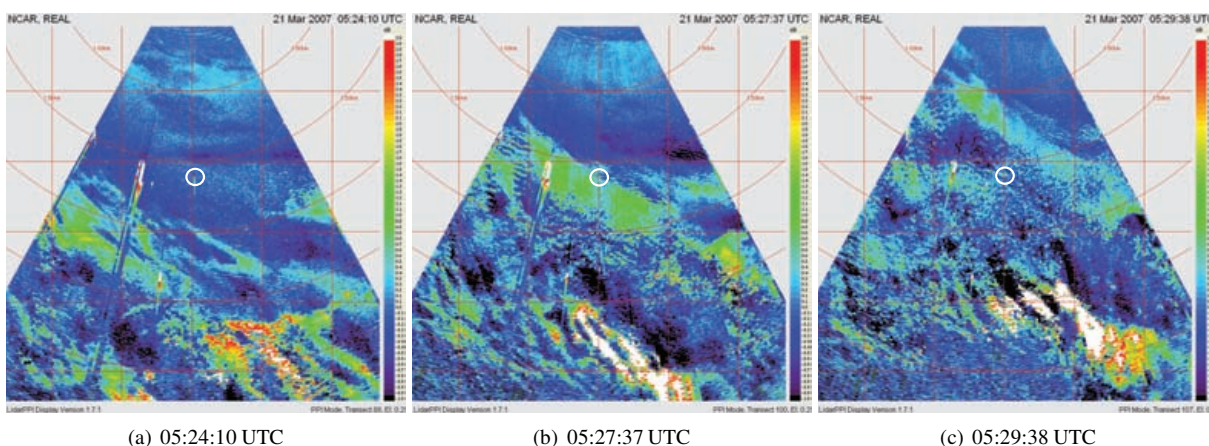

(a) 05:24:10 UTC (b) 05:27:37 UTC (c) 05:29:38 UTC

Figure 10: High-pass median filtered aerosol backscatter from selected near-horizontal scans at 5:24:10, 5:27:37 and 5:29:38 UTC on 21 March 2007. The white circle near the middle indicates the location of the 30 m tall tower.
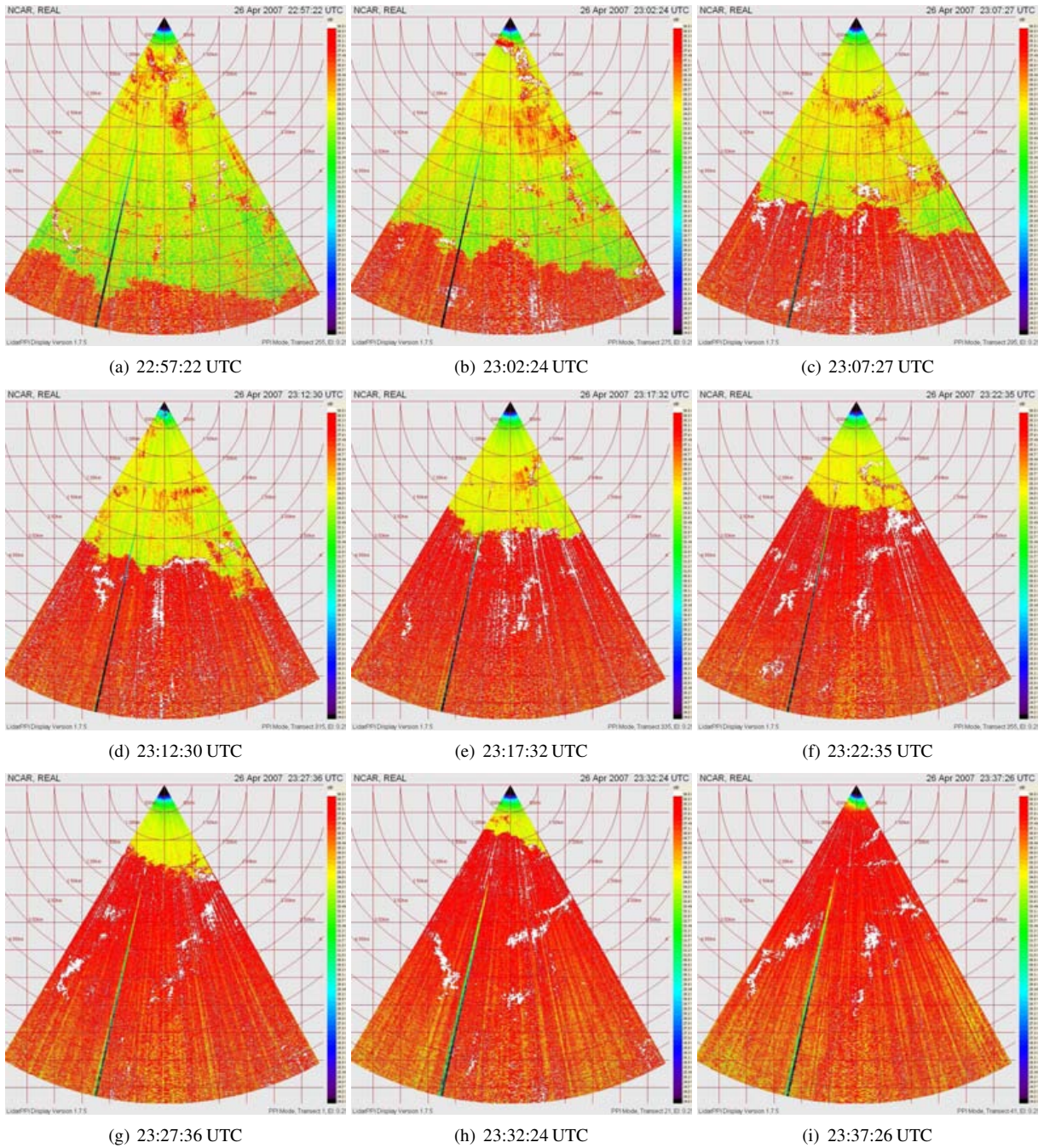
Figure 11: Near-horizontal PPI scans from 22:57:22 UTC to 23:37:26 UTC on 26 April 2007. The elevation angle of the scans is 0.2-degrees above horizontal. Range rings and grid lines are drawn at 500 m intervals. The maximum range shown is 5.8 km.
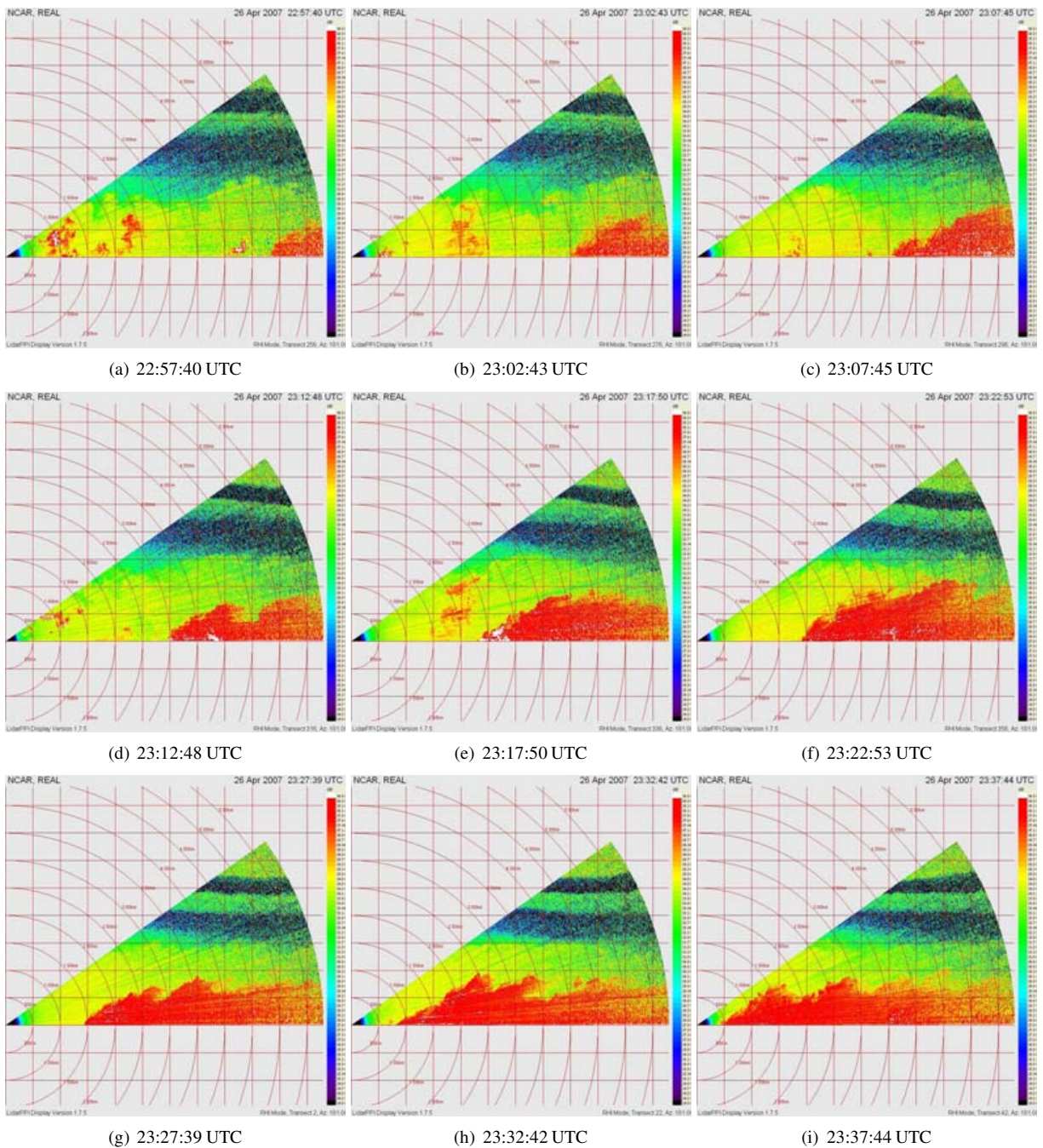
Figure 12: Vertical RHI scans from 22:57:40 UTC to 23:37:44 UTC on 26 April 2007. The azimuth angle is 180-degrees (south). Range rings and grid lines are drawn at 500 m intervals. The maximum range shown is 5.8 km.
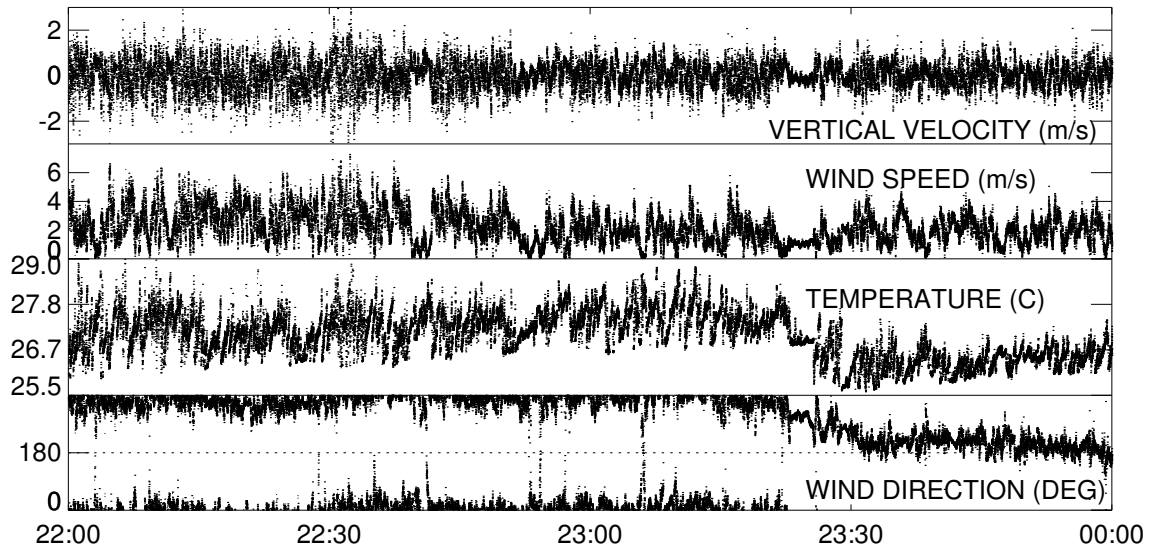
Figure 13: Time series of vertical velocity, horizontal wind speed, temperature, and wind direction collected from in situ sensors on a tower at 12.5 meters above the ground during the passage of the sea-breeze front and shown in Figs. 11 and 12. These 6 Hz data shown were extracted from a 60 Hz time series. The sea-breeze front passed over the tower at approximately 23:27 UTC on 26 April.

4. CONCLUSIONS

The primary question that the experiment set out to answer was "Can elastic lidars be used to create images and time-lapse animations of turbulent coherent structures over the canopy?" In particular, phenomena such as streaks, ejections and sweeps during fair weather conditions. It has been shown in other work that elastic lidars can detect and track turbulent coherent structures during periods of strong dynamics. These included cellular convection (Mayor et al., 2003) and mountain induced phenomena such as waves and rotors (DeWekker and Mayor, 2008). These result in relatively large length scales and large changes in aerosol backscatter intensity. Therefore, the question of whether one can use the elastic lidar to detect very fine scale perturbations depends on three factors: (1) Adequate sensitivity to small changes in aerosol backscatter intensity; (2) Adequate spatial and temporal resolution to detect features on the scales of 10's of meters and tenths of seconds; and (3) air currents inducing small changes in the aerosol backscatter concentration.

To answer these questions, this paper begins exploring the sensitivity of the lidar to small changes in aerosol backscatter (section 3.1) and the spatial and temporal resolution (section 3.2) of the measurements. It appears spatial resolution on the order of 10 meters or less and temporal resolution of approximately 0.1 s can be achieved. It also appears the lidar should be able to detect changes in aerosol backscatter greater than $\pm 6\%$ - $\pm 26\%$ over

ranges of 1 to 4 km range during strong SNR conditions. More work is needed to identify specific features such as ejections and sweeps and the conditions under which they are observable by the lidar.

In addition to enabling the exploration of the goal of observing fine-scale turbulent coherent structures above the canopy, the deployment of REAL at CHATS demonstrates that an elastic lidar can provide unique observations of boundary layer structure and motion. Toward this, examples of fine-scale waves during stable evening conditions and one case of an afternoon sea-breeze front passage was presented. The keys to being able to make these observations are: (1) high single-shot signal-to-noise ratio data, (2) fine spatial and temporal resolution data, (3) eye-safety, and (4) continuous and unattended operation.

5. FUTURE WORK

Much remains to be done. Tasks can be divided into categories of analysis of data already in hand and future experimental field work. Under analysis tasks, the entire data set should be high-pass median filtered and all results (in the form of images) made available on the web. This includes scans and stare periods. Time series of aerosol backscatter at the range bin nearest the tower should be compared with tower variables to determine what variables, other than particle concentration, the aerosol backscatter may be correlated with. Corre-

lation analysis between frames in time should be conducted to derive the motion and lifetimes of aerosol features and these vectors should be compared with wind measurements on the tower. The amount of agreement of the two different types of vectors may be related to the z/L stability parameter at the altitude of comparison. The CHATS data set provides an ideal opportunity to determine under what stability conditions, and to what accuracy, the lidar correlation wind technique works and fails.

A thorough analysis of the observations of sea-breeze fronts also should be completed. In addition to applying correlation techniques to derive the vector motion field, wavelet techniques could be applied to the lidar scans to objectively locate and track the leading edge of the front. The lidar data is uniquely capable of revealing structure of the front such as slope of the nose where the leading edge intersects the surface, billow characteristics such as amplitude and spacing, airmass depth, and lobe and cleft structure of the leading edge in the horizontal dimension. These features and the speed the front can be used to test present theoretical understanding of atmospheric density currents.

Future field experiments should focus on operating REAL simultaneously with in situ instrumentation capable of determining the microphysical properties of the atmospheric aerosol. This would include size-resolved particle concentration and relative humidity. Sensitivity tests should be conducted to determine how REAL responds to small changes in concentration of specific types of common aerosols—including fine particles. Because REAL is eye-safe, the beam can be directed horizontally near ground level and aerosols can be safely injected into the beam at a distance to determine sensitivity. Finally, a study should be conducted to determine how well the instrument can detect and monitor atmospheric boundary layer depth.

REFERENCES

DeWekker, S. F. J. and S. D. Mayor, 2008: Observations of atmospheric structure and dynamics in the owens valley of california with a ground-based, eye-safe, scanning aerosol lidar, *J. Clim. Appl. Meteor.*, Submitted.

Eloranta, E. W., J. M. King, and J. A. Weinman, 1975: The determination of wind speeds in the boundary layer by monostatic lidar, *J. Appl. Meteor.*, **14**, 1485–1489.

Kunkel, K. E., E. W. Eloranta, and J. Weinman, 1980: Remote determination of winds, turbulence spectra and energy dissipation rates in the boundary layer from lidar measurements, *J. Atmos. Sci.*, **37**, 978–985.

Mayor, S. D. and E. W. Eloranta, 2001: Two-dimensional vector wind fields from volume imaging lidar data, *J. Appl. Meteor.*, **40**, 1331–1346.

Mayor, S. D. and S. M. Spuler, 2004: Raman-shifted eye-safe aerosol lidar (REAL), *Appl. Optics*, **43**, 3915–3924.

Mayor, S. D., S. M. Spuler, and B. M. Morley, 2008: Raman-shifted eye-safe aerosol lidar, in *Symposium on Recent Developments in Atmospheric Applications of Radar and Lidar*, AMS.

Mayor, S. D., S. M. Spuler, B. M. Morley, S. C. Himmelsbach, R. A. Rilling, T. M. Weckwerth, E. G. Patton, and D. H. Lenschow, 2007a: Elastic backscatter lidar observations of sea-breeze fronts in Dixon, California, in *7th Conf. on Coastal Atmospheric and Oceanic Prediction and Processes*, AMS.

Mayor, S. D., S. M. Spuler, B. M. Morley, and E. Loew, 2007b: Polarization lidar at 1.54-microns and observations of plumes from aerosol generators, *Opt. Eng.*, **46**, DOI: 10.1117/12.781902.

Mayor, S. D., G. J. Tripoli, and E. W. Eloranta, 2003: Evaluating large-eddy simulations using volume imaging lidar, *Mon. Wea. Rev.*, **131**, 1428–1452.

Sasano, Y., H. Hirohara, T. Yamasaki, H. Shimizu, N. Takeuchi, and T. Kawamura, 1982: Horizontal wind vector determination from the displacement of aerosol distribution patterns observed by a scanning lidar, *J. Appl. Meteor.*, **21**, 1516–1523.

Spuler, S. M. and S. D. Mayor, 2005: Scanning eye-safe elastic backscatter lidar at 1.54 microns, *J. Atmos. Ocean. Technol.*, **22**, 696–703.